 doi:10.20944/preprints202107.0672.v1

Research paper

Application of the Generalized Nonlinear Constitutive Law to Hollow-Core Slabs

N. Staszak[1], T. Garbowski[2], B. Ksit[3]

Abstract: The non-linear analysis of hollow-core concrete slabs requires the use of advanced numerical techniques, proper constitutive models both for concrete and steel as well as particular computational skills. If prestressing, cracking, crack opening, material softening, etc. are also to be taken into account, then the computational task can far exceed the capabilities of an ordinary engineer. In order for the calculations to be carried out in a traditional design office, simplified calculation methods are needed. Preferably based on the linear finite element (FE) method with a simple approach that takes into account material nonlinearities. In this paper the simplified analysis of hollow-core slabs based on the generalized nonlinear constitutive law is presented. In the proposed method a simple decomposition of the traditional iterative linear finite element analysis and the non-linear algebraic analysis of the plate cross-section is used. Through independent analysis of the plate cross-section in different deformation states, a degraded plate stiffness can be obtained, which allows iterative update of displacements and rotations in the nodes of the FE model. Which in turn allows to update the deformation state and then correct translations and rotations in the nodes again. The results obtained from the full detailed 3D nonlinear FEM model and from the proposed approach are compared for different slab cross-sections. The obtained results from both models are consistent.

Keywords: generalized nonlinear constitutive law, finite element analysis, nonlinear materials, composite structures, Reissner-Mindlin plate element

[1] MSc., FEMat Sp. z o.o., R&D Department, Romana Maya 1, 61-371, Poznan, Poland, e-mail: natalia.staszak@fematproject.pl, ORCID: 0000-0001-8960-9573

[2] PhD., Assoc. Prof., Poznan University of Life Sciences, Department of Biosystems Engineering, Wojska Polskiego 50, 60-627 Poznan, Poland, e-mail: tomasz.garbowski@up.poznan.pl, ORCID: 0000-0002-9588-2514

[3] PhD., Poznan University of Technology, Institute of Building Engineering, Piotrowo 5, 60-965 Poznan, Poland, e-mail: barbara.ksit@put.poznan.pl, ORCID: 0000-0001-6459-8783

 doi:10.20944/preprints202107.0672.v1

1. Introduction

The prefabricated ceilings, including prestressed multi-channel slabs belong to the family of floors with the largest span. Prestressed hollow core slabs (PHCS) are one of the most popular type of prefabricated floor used in civil engineering. They are used in industrial as well as in residential constructions. In Poland, this kind of ceiling were introduced under the name PS ("Prestressed Slab") in 1973-76 on the basis of a licence for Spiroll ceilings. In the world this type of ceiling is known under the trade names Elematic Dy-core Rap Soprel [4]. The first hollow core ceilings with a height of 22 centimetres were used for a span of 6,0 meters, while the prestressed type Spiroll ceiling with a height of 26.5 cm were produced up to a span of 12 meters. Currently, the ceilings are manufactured with a wide range of prestressing reinforcement grades, which allows them to be used for various loads and slab lengths from 3.0 m to 20.7 m and heights from 16 to 50 cm. In the case of PHCS slabs the span can reach up to 26 m as stated by the manufacturer [24]. It is extremely important nowadays that the PS ceilings can be considered as building elements supporting sustainable construction [5]. This is because for the production of prestressed structures, the amount of concrete and steel needed is significantly reduced compared to reinforced concrete structures, making this structures more environmentally friendly. Thanks to this, the amount of greenhouse gases emitted, including CO_2 is again reduced [7].

Another advantage, this time related to carrying capacity parameters and limit states, is lower deflection of prestressed slabs than of reinforced concrete floors at the same loads. It is the result of the 'lifting' action of the appropriately profiled tendons. An additional factor influencing the differences in deflection of reinforced and prestressed concrete floors is material creep. This phenomenon causes an increase in floor deflection with time in the presence of long-term loads. The self-weight of the floor is such a long-term load acting constantly over time. In the case of prestressed floors, there are also other long term loads, namely cable forces that push the floor upwards. These forces act counter to the weight in the centre of the floor, thus reducing the long-term creep deformation of the concrete. It should also be noted that prestressing minimizes the possibility of cracking and fracture in the concrete, thus sealing the floor and protecting the reinforcement against the corrosive effects of the external environment [31, 32, 34].

The great advantage of using prestressed prefabricated slabs is the reduction of wet work on the construction site and acceleration of the task implementation. The technology of making such ceilings is characterized by quick assembly on the construction site. There is no need for additional supports

 doi:10.20944/preprints202107.0672.v1

or formwork during assembly, which results in a smooth and even bottom surface. Another advantage of using such slabs is the freedom in arranging partition walls.

These ceilings, however also have disadvantages. One of the main disadvantage is its cost, the slabs themselves are relatively expensive and a crane has to be used for assembly [26]. However, this is usually not a problem because heavy equipment is frequently available on a large construction sites, where those slabs are often applied. Additionally, not all prestressed slabs should be handled with heavy equipment, e.g. PHCS type floor slabs (prestressed hollow core slabs) weighing 150 kilograms can be handled with a traverse or hook sling attached to a light HDS crane. Another danger is water getting inside the floor system duct. In order to eliminate a possible risk of ceiling slab damage as a result of frozen water in channels, the manufacturers suggest to make holes in the bottom of the slab at the distance of approximately 50 centimetres from the support in order to drain possible water that collects in the slab's channels.

Prestressed slabs can be shaped in many ways to suit the local conditions that are most common in the designed buildings. Slabs can be shaped by cutting longitudinally or transversely and by making cuts and holes according to specified rules. It is extremely important to plan all openings as early as the design stage, i.e. before selecting the location of the prestressed cables. Achieving optimal strength parameters of floor slabs is possible with various variants of the arrangement of the tendons on the floor plan. After the ceiling is formed, it is very difficult to make new openings [9].

The typical design of such structures is relatively easy thanks to the possibility of direct use of technical catalogues published by its manufacturers. However, for a more advanced nonlinear analysis of the strength of the slabs, such as the ceiling with openings, this simplified approach may not be sufficient [3, 18] and therefore it is often necessary to support the design with a detailed numerical model. Additionally, it is very tedious to use the formulas available in international standards, such as [25]. Deep insight into the nonlinearity of the steel and the inhomogeneity of the concrete and sometimes complex geometry is only possible with a numerical modelling. One may use here the popular finite element method (FEM) [13, 14, 27, 28, 29], which is able to give the correct solution, if the model uses robust input data and the modelling approach is adequate. Note that, the detailed FEM modelling for complex slab structures may be computationally (time) expensive and requires specialized knowledge.

In the literature one can find many experimental and computational examples, in which prestressed hollow-core concrete slabs are analysed. For example, in the work [16] the hollow-core slabs were subjected to experimental tests. Information on the puncture resistance of concrete plates can be found

Preprints (www.preprints.org) | NOT PEER-REVIEWED | Posted: 29 July 2021 doi:10.20944/preprints202107.0672.v1

in the paper [6]. In turn, both experimental and numerical studies were carried out in the works [2, 15, 19].

This paper focuses on advanced numerical analysis of prefabricated, prestressed concrete slabs. The presented method uses the classical linear finite element method extended by a generalized non-linear constitutive law (GNCL), which allows for nonlinear material modelling of both steel and concrete. The main goal is to achieve great practicality of the proposed method, therefore it bases on a simple and generally available FE algorithm for linear analysis of prefabricated slabs. This allows to obtain quick and precise results of geometrically complex and multi-material plate sections without the need to use advanced software. The proposed method also takes into account the sequential application of both prestressing and permanent loads. In order to validate the presented method, a full 3D model was also built in a commercial software. Satisfactory compliance of the results obtained by the GNCL method and the detailed full 3D FE model for the selected geometries of the prestressed slabs was obtained.

2. General nonlinear constitutive law

2.1. Normal strain and curvature

The computational method using generalized nonlinear constitutive law can be divided into two main parts. The first part consists of the standard procedures based on the finite element method presented in this chapter. In the second part, the cross-section of analysed structure is homogenized and generalized constitutive law is formulated. The GNCL can be easily embedded in FE analysis and thus becomes an integral part of classical FE analysis. In this work, attention is paid to hollow-core slabs loaded by external forces and/or displacements in the small strains and deformations regime. The proposed method is an iterative method, in which the bending stiffness of the analysed element is changed iteratively. In each of the n-th iterations, calculate the nodal displacements d^n. Figure 1 and Figure 2 show the block diagrams of the both stages in the computational algorithm of the proposed methods.

In the classical FE method, the global stiffness matrix is formed by summing the individual stiffness matrices of all elements. In contrast to classical linear method, in the proposed method, the stiffness of the element is modified (through the application of GNCL) by iterative reduction of the elastic stiffness during the analysis due to deformations (normal strains ε_0 and curvature κ). Each of these deformations is calculated from the nodal displacements d. Since prestressed slabs have a relatively

Preprints (www.preprints.org) | NOT PEER-REVIEWED | Posted: 29 July 2021 doi:10.20944/preprints202107.0672.v1

small ratio of width to length and height to length, and they are also mainly bent in one direction, a beam model can be used for their analysis. In such models the normal deformation is calculated from:

$$\varepsilon_0 = \frac{\Delta L}{L} = \frac{u_2 - u_1}{L}, \tag{2.1}$$

where ΔL is the element elongation, L is a beam length, u_1, u_2 are the nodal displacements along the beam axis.

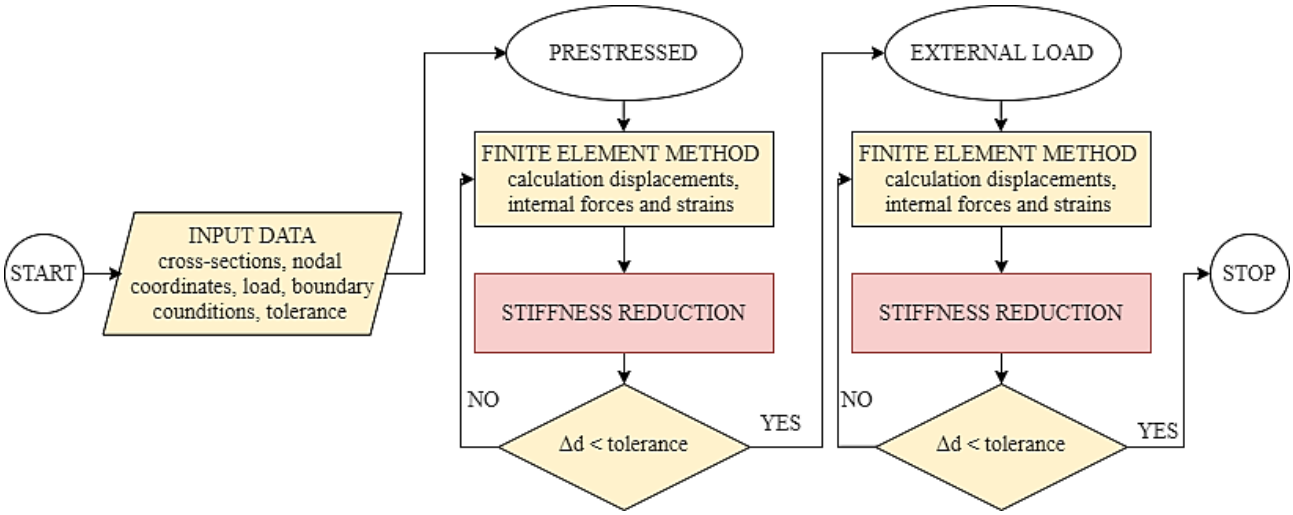

Fig. 1. Block diagram of the computational algorithm of the GNCL methods.

The curvature, κ, is obtained from the beam deflection function $v(x)$. While the deflection of the beam is assumed as a third degree polynomial:

$$v(x) = C_3 x^3 + C_2 x^2 + C_1 x + C_0 . \tag{2.2}$$

Based on the boundary conditions, polynomial constants can be determined. In case of beams the following boundary conditions can be assumed:

$$\begin{aligned} x = 0, \quad v(0) = v_1, \quad \frac{\mathrm{d}v(0)}{\mathrm{d}x} = \varphi_1 , \\ x = L, \quad v(L) = v_2, \quad \frac{\mathrm{d}v(L)}{\mathrm{d}x} = \varphi_2 . \end{aligned} \tag{2.3}$$

Thanks to this we obtain the following coefficients of the beam deflection function:

Preprints (www.preprints.org) | NOT PEER-REVIEWED | Posted: 29 July 2021 doi:10.20944/preprints202107.0672.v1

$$C_0 = v_1\,, \qquad C_2 = \frac{3(v_1+v_2)+(2\varphi_1+\varphi_2)L}{L^2}\,,$$
$$C_1 = \varphi_1\,, \qquad C_3 = \frac{2(v_1+v_2)+(\varphi_1+\varphi_2)L}{L^3}\,. \tag{2.4}$$

Knowing these coefficients, deflection function, $v(x)$, can be determined. It enables the calculations of the curvature. When the displacements are small, the following simplification of the curvature calculations can be assumed:

$$\kappa(x) = \frac{\mathrm{d}^2 v}{\mathrm{d}x^2}\,. \tag{2.5}$$

After this simplification, the curvature has the form:

$$\kappa(x) = -\frac{2}{L^3}\left[\varphi_1 L(2L-3x)+\varphi_2 L(L-3x)+3(v_1-v_2)(L-2x)\right]. \tag{2.6}$$

The effective curvature is used in the presented approach. That is, the weighted mean curvature, $\bar{\kappa}$, which can be calculated in three Gauss points:

$$\bar{\kappa} = B_1\kappa_1 + B_2\kappa_2 + B_3\kappa_3\,, \tag{2.7}$$

where B_1, B_2, B_3 are weights, which takes the values: $B_1 = 5/18$, $B_2 = 4/9$ and $B_3 = 5/18$. The curvatures $\kappa_1, \kappa_2, \kappa_3$ are calculated in the following three Gaussian point locations: $x_1 = 1/9\,L$, $x_2 = 1/2\,L$, and $x_3 = 8/9\,L$.

2.2. Stiffness reduction

In Figure 1 and Figure 2 the general algorithm of the method proposed in this article in the form of flowcharts are shown. It is an extension of the method proposed by Szumigała [33] later modified by [22, 23, 30]. The previous approaches were applied to beams [33], 2D flexural beams [22], steel frames [23] and trapezoidal steel sheets [30], while here it is extended to prestressed ceiling structures. The main modifications concern: (1) the possibility of considering the actual hole geometry; (2)

Preprints (www.preprints.org) | NOT PEER-REVIEWED | Posted: 29 July 2021 doi:10.20944/preprints202107.0672.v1

including the GNCL procedure in the main calculation procedure; (3) considering prestressed reinforcement and (4) introducing a sequential load, which allows to analyse the stiffness degradation history. In the original method, a cross-section analysis was done prior to the main calculations. Then, during the main analysis, the stiffness values of all finite elements were obtained by interpolating the preliminary computed values. With that approach the accuracy of the calculations depends on the adopted discretization density. Proposed modification of the method allows the cross-section analysis during the calculations within iteration loop, thus, gives actual results and, therefore, interpolation errors are avoided.

Here, as in the original method, the cross-section of the analysed element is divided into horizontal, thin strips. Based on the strain and curvature of the elements (ε_0 and κ), which were derived in the previous subsection 2.1, the degradation in stiffness can be calculated. For each layer, the geometric properties, i.e. position, width, height and cross-sectional area of individual materials, are specified separately. This operation is repeated for all materials and each strip.

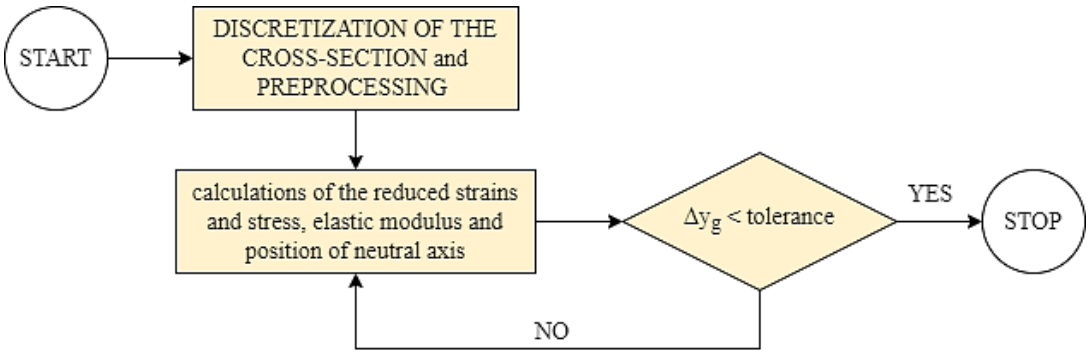

Fig. 2. Block diagram of stiffness reduction function.

After determining the geometric properties, the reduced strains (ε_{red}) are calculated by considering the normal strains:

$$\varepsilon_{red} = \varepsilon_x = \kappa(y_g - y_i) + \varepsilon_0, \tag{2.8}$$

where: ε_x is normal strains, y_g and y_i are position of neutral axis of the whole section and the i-th layers relative to its top edge, respectively. Next, the reduced stress (σ_{red}) in the each layer is calculated based on the theoretical stress-strain relationship for a chosen material. The effective stresses are determined for each material, if the cross-section consists of several materials. Then,

Preprints (www.preprints.org) | NOT PEER-REVIEWED | Posted: 29 July 2021 doi:10.20944/preprints202107.0672.v1

based on the computed strains and stresses values, the Young's modulus (E) is calculated by the following formula:

$$E = \frac{\sigma_{red}}{\varepsilon_{red}}. \tag{2.9}$$

In the following step, the tensile stiffnesses can be computed:

$$B_N = \sum_{j=1}^{n}\sum_{i=1}^{m} {E_i}^j \, {A_i}^j, \tag{2.10}$$

where j and i specify the material and the layer number in the cross-section, respectively; m and n are the total number of layers and number of materials, respectively. ${E_i}^j$ and ${A_i}^j$ are a Young's modulus and a cross-section area of j-th material and i-th layer, respectively.

A position of the neutral axis in k-th iteration of calculation, ${y_g}^k$, may be determined according to the expression:

$${y_g}^k = \frac{\sum_{j=1}^{n}\sum_{i=1}^{m} {E_i}^j \, {A_i}^j \, y_i}{EA}. \tag{2.11}$$

Knowing the position of the neutral axis, it is possible to calculate the moment of inertia of i-th layer, ${I_i}^j$. Thus, the bending stiffness, B_M, is obtained from:

$$B_M = \sum_{j=1}^{n}\sum_{i=1}^{m} {E_i}^j \, {I_i}^j \, . \tag{2.12}$$

2.3. Constitutive models

In the proposed method the nonlinear constitutive law of material can be easily embedded in the FE procedure. Here the nonlinear constitutive law both for steel and concrete is assumed. Table 1 summarizes the engineering parameters of the materials used in the performed tests, where E is the Young's modulus, ν is Poisson's ratio, ρ is density, $f_{p,0.1,k}$ is the yield strength of prestressed steel,

Preprints (www.preprints.org) | NOT PEER-REVIEWED | Posted: 29 July 2021 doi:10.20944/preprints202107.0672.v1

f_{cm} is the average value of the concrete compressive strength and f_{ctk} is a characteristic value of a tension strength of concrete.

Table 1. Material parameters of concrete and prestressed steel used in the tests.

Material	E [GPa]	ν [−]	ρ [kg/m^3]	$f_{p,0.1,k}$ [MPa]	f_{cm} [MPa]	f_{ctk} [MPa]
prestressed steel	195.0	0.3	7900	1674.0	–	–
concrete	35.0	0.2	2400	–	48.0	2.5

The concrete is described by a nonlinear behaviour, which in a simplified way reflects the relationship presented in [25]. Additionally, the tensile strength of concrete was taken into account in the analyzes. In order to verify the obtained results, also the commercial software, i.e. Abaqus FEA [1] was used (the description of the FE models can be found in the results section). The following nonlinear concrete model presented in Eurocode 2 was used in the benchmark examples:

$$\frac{\sigma_{red}}{f_{cm}} = \frac{k\eta - \eta^2}{1 + (k+2)\eta}, \tag{2.13}$$

where $\eta = \varepsilon_c/\varepsilon_{c1}$ and k is computed as

$$k = 1{,}05E_b\frac{\varepsilon_{c1}}{f_{cm}}, \tag{2.14}$$

while ε_{c1} is the deformation corresponding to the greatest stress and is taken for different grades of concrete from Eurocode 2.

A number of different constitutive models for concrete can be used in the computational analysis, e.g. the classical Drucker-Prager model [8], which is relatively easy to be calibrated, see e.g. [11, 12, 21]. Here, however the concrete damage plasticity (CDP) model was used to take into account both compression and tension nonlinear behaviour of concrete. This model can be calibrated using the procedure described by Jankowiak & Łodygowski [17] or by Gajewski & Garbowski [10].

An elastic perfectly-plastic model was used to describe the behaviour of prestressed steel:

Preprints (www.preprints.org) | NOT PEER-REVIEWED | Posted: 29 July 2021 doi:10.20944/preprints202107.0672.v1

$$\sigma_{red} = \begin{cases} E_p \varepsilon_{red}, & \text{for} \quad \varepsilon_{red} < \dfrac{f_{p,0.1,k}}{E_p}, \\ f_{p,0.1,k} & \text{for} \quad \varepsilon_{red} \geq \dfrac{f_{p,0.1,k}}{E_p}, \end{cases} \tag{2.15}$$

Table 1 presents the material parameters of prestressed steel and concrete. While Table 2 shows the constitutive properties used in the CDP model.

Table 2. Material properties of concrete used in the reference models.

Elastic		Concrete Damage Plasticity				
E [GPa]	ν [−]	Dilation Angle [°]	Eccentricity [−]	f_{b0}/f_{c0} [−]	K [−]	Viscosity Parameter [−]
35.0	0.2	38	0	1.16	0.667	1e-6

2.3. Benchmark models

In order to verify the proposed FE-GNCL method, two examples were computed via in-house algorithm implemented in MATLAB [20]. Then, the obtained deflections using the presented method were compared with the results obtained from the model built in the commercial software ABAQUS FEA [1]. In all benchmark examples, the slabs freely supported on two opposite sides were analysed. They were prestressed first and then a uniformly distributed load was applied to the upper surface of the slab (see Figure 3). When using ABAQUS FEA, abbreviated to FE-ABQ the slabs were modelled as a three-dimensional structure, while in the case of the FE-GNCL the model was simplified to a beam structure.

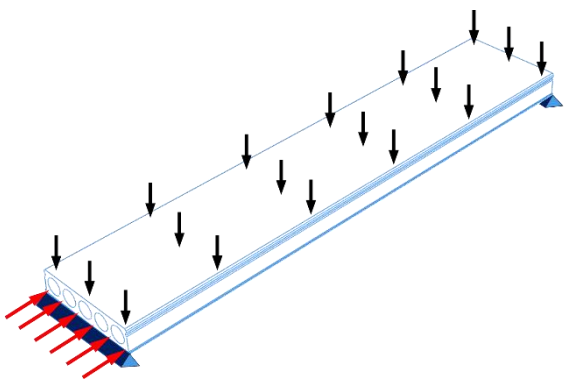

Fig. 3. Loads and boundary conditions of channel prestressed concrete slab.

Preprints (www.preprints.org) | NOT PEER-REVIEWED | Posted: 29 July 2021 doi:10.20944/preprints202107.0672.v1

In Model 1, typical hollow core slab PHC 26.5-6 was analysed. It was 6.00 meters long and 265 mm high. The slab also had 5 circular holes with diameter 180 mm. The hollow-core slab was reinforced with 6 tendons with diameter of 12.5 mm. The cross-section of the slab in FE-ABQ model corresponded to the actual slab cross-section (see Figure 4a). However, in the case of the FE-GNCL model, the cross-section was simplified to the rectangular external contour (see Figure 4b).

Figure 4 shows both the exact and simplified cross-sections of the slab. The adopted simplification of the cross-section did not significantly affect the results; the difference was a maximum of 0.3%.

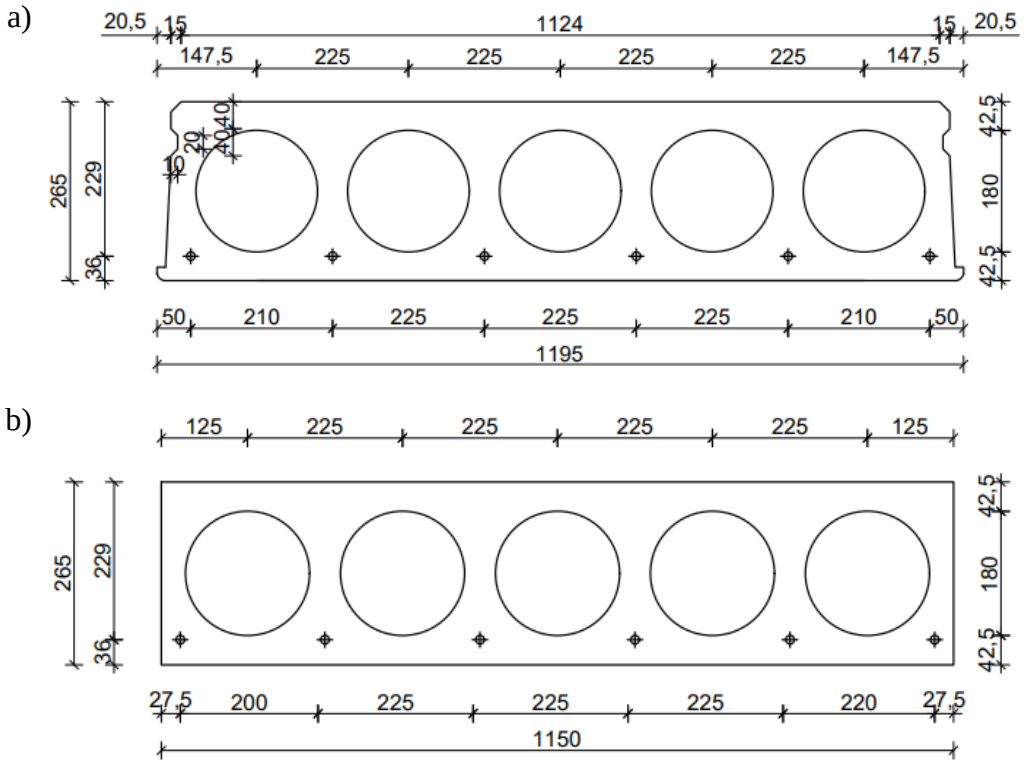

Fig. 4. Cross-section of plate PHC 26.5-6: (a) real; (b) simplified.

As already mentioned, in FE-ABQ model the slab was modelled as a three-dimensional concrete structure. The reinforcement, on the other hand, was modelled as a steel bar structure. Additionally, the tendons were anchored in the concrete slab using the built-in techniques available in the Abaqus. The model was prestressed by a force with a value of 1674 MPa per a single truss. Then, a uniformly distributed load of 45.0 kN/m^2 was applied to the upper surface of the slab.

The concrete cross-section was divided into 3D solid elements with dimensions of 40 mm in the width and height of the cross-section and 80 mm in the length of the slab. As a result, 11,250 elements with 20 nodes and 3 degrees of freedom in each node were obtained , see Figure 5. Such elements are called C3D20R according to [1] and are implemented within the reduced integration scheme. The

Preprints (www.preprints.org) | NOT PEER-REVIEWED | Posted: 29 July 2021 doi:10.20944/preprints202107.0672.v1

tendons were divided by means of two-node truss elements with 3 degrees of freedom (T3D2 according to [1]) with a length of 150mm. This gives in total 240 elements. So a total number of 11,490 elements was used in the calculations. Consequently, the total number of nodes in model I was 225,480, which translates to 676,440 total degrees of freedom.

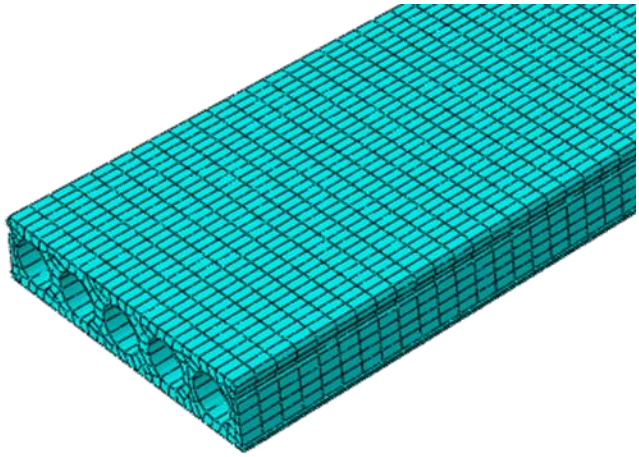

Fig. 5. Discretization of the hollow-core slab PHC 26.5-6.

In the case of the FE-GNCL model used for calculations in MATLAB [20] subroutine, the stiffness in the cross direction was assumed to be much higher than in longitudinal direction, therefore slab was treated as a beam. The slab was prestressed by a force corresponding to the prestress value from the 3D reference model, and then a uniformly distributed load of 50.5 kN/m was applied This value is equivalent to the applied external load in FE-ABQ model.

a)

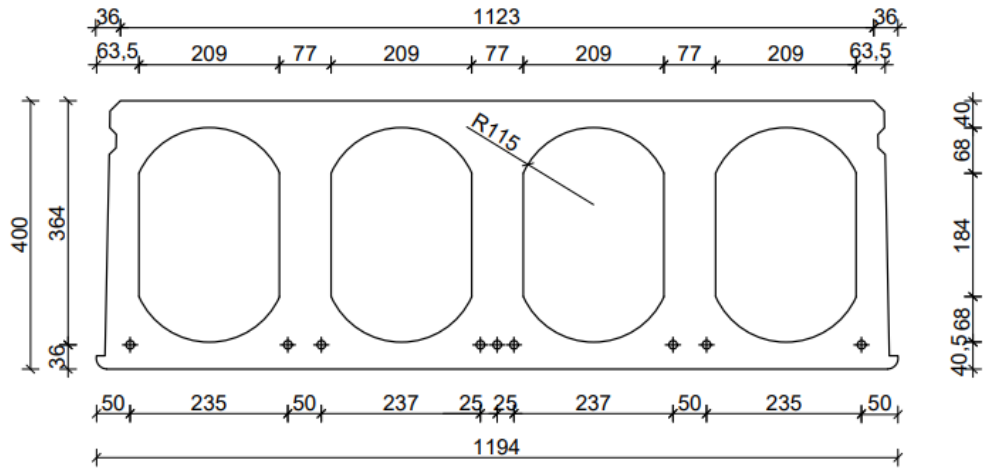

Preprints (www.preprints.org) | NOT PEER-REVIEWED | Posted: 29 July 2021 doi:10.20944/preprints202107.0672.v1

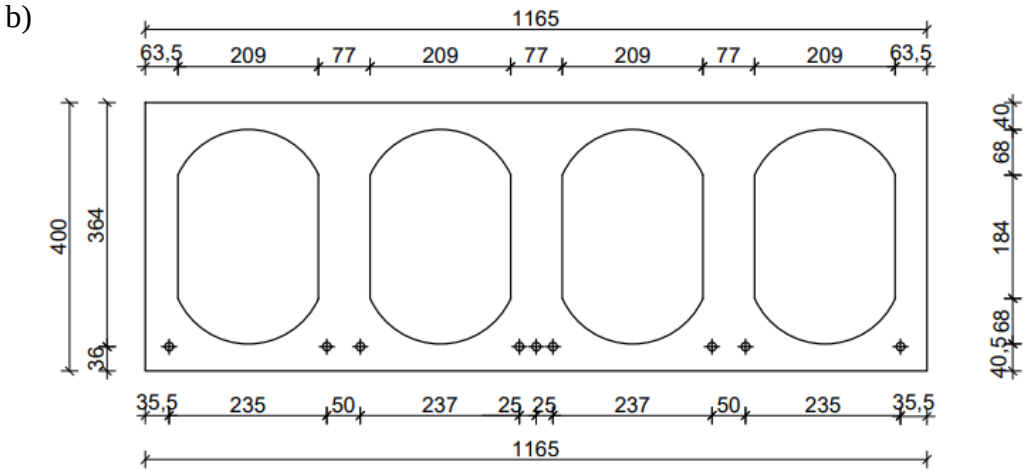

Fig. 6. Cross-section of plate PHC 40.0-9: (a) real; (b) simplified.

In the second example, a standard hollow core slab PHC 40.0-9 was considered. The 15.00 m long and 400 mm high hollow core slab was considered. There were 4 elongated channels in the slab, evenly spaced across the slab's cross-section. Additionally, the plate has bottom reinforcement in the form of 9 tendons with a diameter of 12.5 mm. In the numerical FE-ABQ model, the actual slab cross-section shown in Figure 6a was used. While the FE-GNCL model uses a simplified rectangular cross-section (see Figure 6b).

Similar to the previous example the numerical model in Model 2 was built in the ABAQUS FEA [1]. The 40.0-9 slab was modelled as a three-dimensional concrete structure reinforced with tendons. Additionally the reinforcement was modelled as bar structures made of prestressing steel. Thanks to the available functionality in the Abaqus, the bars were embedded in the concrete part of the numerical model. The prestress of 921 kN was introduced into the slab, causing the slab to bend. The next a uniformly distributed load of values 5.4 kN/m^2 was applied to the slab.

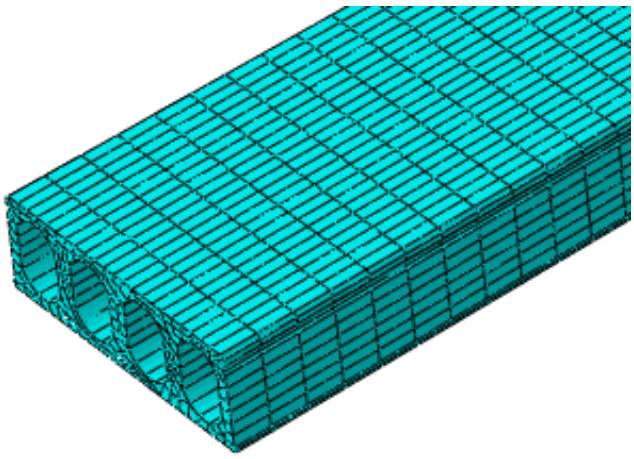

Fig. 7. Discretization of the channel panel PHC 40.0-9.

Preprints (www.preprints.org) | NOT PEER-REVIEWED | Posted: 29 July 2021 doi:10.20944/preprints202107.0672.v1

The concrete part of the reference model II, similar to I, was discretized with the use of 3D solid elements (C3D20R according to [1]), while the bars with the use of truss elements (T3D2 according to [1]). The slab was divided into 16,400 elements with the following dimensions: 50 mm in height and width and 150 mm along the slab (see Figure 7), while each strand into 100 elements 150 mm long. Model II consists of 17,750 elements and 356,800 nodes. As a result, 1,070,400 degrees of freedom were obtained (each node consists of 3 degrees of freedom).

In the FE-GNCL model, a simplification was taken and the slab was treated as a beam assuming that the stiffness of the slab in the cross direction is much greater than in the longitudinal direction. Also in this case, the prestressed force was applied on a certain eccentricity and with the same value as that used in the reference model. Later, the slab was subjected to a uniformly distributed load of 6 kN/m.

3. Results and discussion

3.1. Example I

In Figures 8 and 9, the results of the numerical analysis for the full three-dimensional numerical model for prestress and for combined action of prestress and external load are shown. Figure 8 presents a side view of the plate subjected to a prestress force only. The upward deflection of 8.641 mm was obtained.

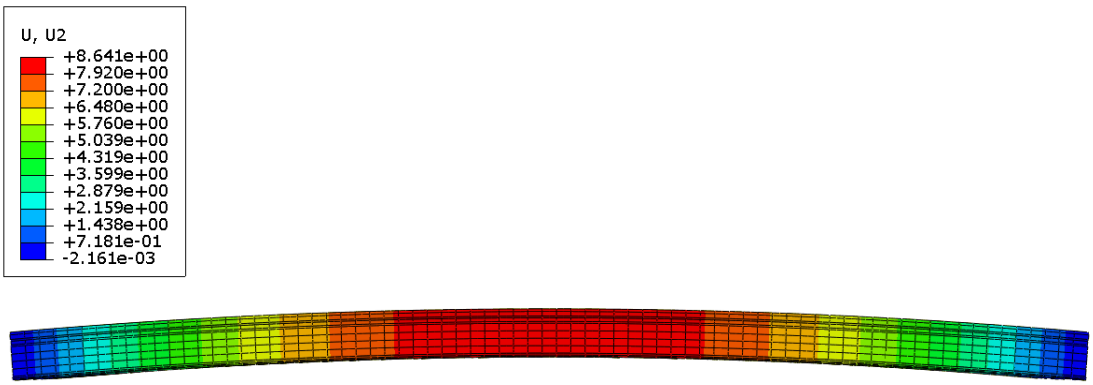

Fig. 8. Vertical displacement of the plate PHC 26.5-6 due to prestress.

In the case of the simultaneous action of a load evenly distributed over the upper surface and the prestress of the slab, the maximum vertical displacement of 10.80 mm was obtained (see Figure 9).

Preprints (www.preprints.org) | NOT PEER-REVIEWED | Posted: 29 July 2021 doi:10.20944/preprints202107.0672.v1

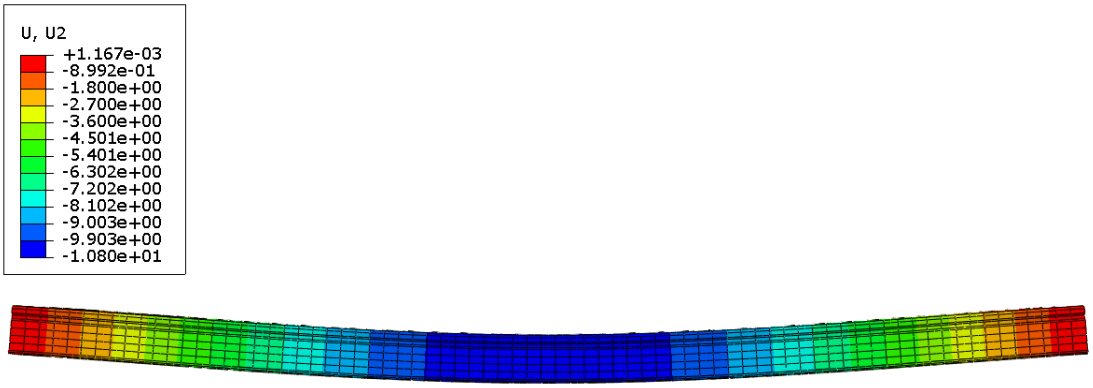

Fig. 9. Vertical displacement of the plate PHC 26.5-6 due to prestress and external load.

Due to the prestressing of the structure, smaller displacements were obtained than for the non-prestressed case. It is caused by the emerging initial upward deflection of the model. As a result of the performed calculations using the FE-GNCL model, the final diagram of the element stiffness under stress and external load was obtained (see Figure 10).

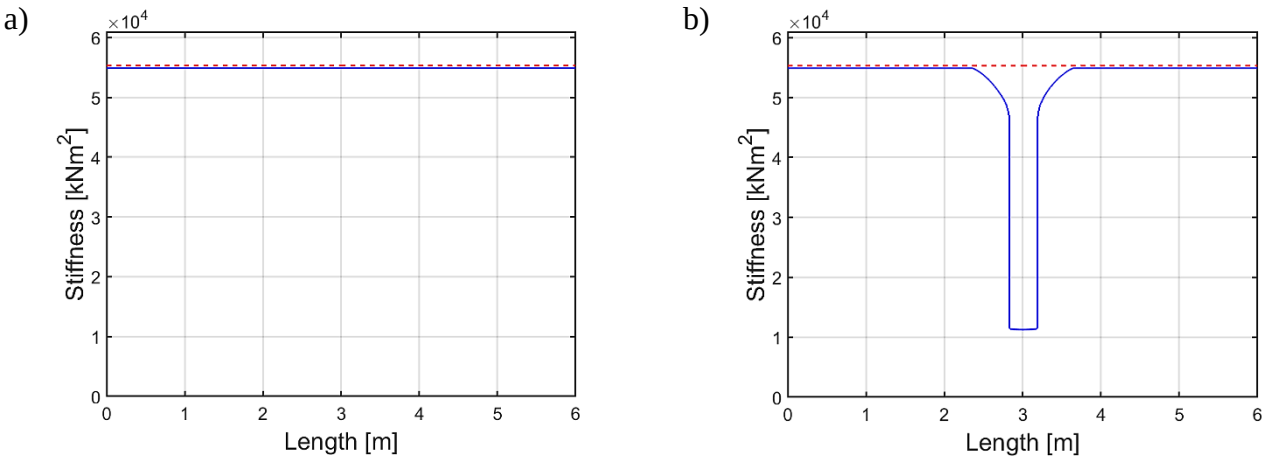

Fig. 10. The stiffness of the elements along the length of the plate PHC 26.5-6 due to:
(a) prestress, (b) prestress and external load.

The red lines show the values of stiffness (Figure 10) and vertical displacements (Figure 11) for the slab with constant stiffness ($EI = \text{const}$), while the blue lines represent the values after taking into account changes in stiffness occurring along the slab length. In the case of prestressing, a minimum decrease in stiffness of about 0.8% was obtained in the entire section of the slab. However, in the case of prestressing and the action of external load, there was a significant drop in stiffness. The maximum decrease was even 80%; it can be observed in the middle of the slab span. This is due to the nonlinearity of the materials used in the analysis.

Preprints (www.preprints.org) | NOT PEER-REVIEWED | Posted: 29 July 2021 doi:10.20944/preprints202107.0672.v1

The vertical plate displacements obtained from the GNCL model are shown in Figure 11. The maximum vertical displacement due to prestressing and external load is 10.81 mm. On the other hand, from the prestress itself, the negative deflection is equal to 8.748 mm.

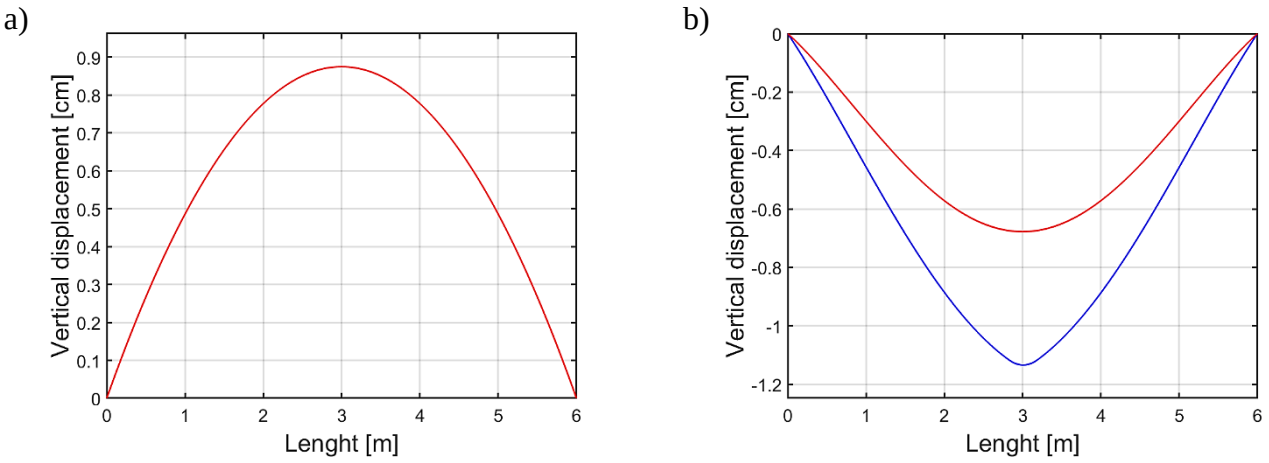

Fig. 11. Vertical displacement of the plate PHC 26.5-6 due to:
(a) prestress, (b) prestress and external load.

From Figure 11b, it can be concluded that the use of nonlinear analysis causes that the vertical displacements of the slab increases. The displacements increased by 69% in relation to the displacements obtained in the elastic range. Table 3 summarizes the obtained results of the maximum vertical displacements from the reference numerical model and GNCL model.

Table 3. Maximum vertical displacements of the plate PHC 26.5-6.

	Reference model	GNCL model
Vertical displacement due to prestress [mm]	-8.641	-8.748
Vertical displacement due to prestress and external load [mm]	10.80	11.120

The obtained vertical displacements from the reference model and the GNCL model differ by 1.2% for prestressing and by 2.9% for the combined action of prestress and external load. Additionally, on the basis of the Consis catalog [24], the initial upward deflection coming from the applied prestress for the PHC 26.5-6 plate is 8.4 mm, which is very close to the results obtained from both models. The development of a numerical reference FE-ABQ model and calculation took much longer time than analysis with the FE-GNCL model. Thus, the use of the model based on cross-section homogenization seems to be more advantageous, because the calculations with GNCL algorithm are much faster and the obtained results are consistent with advanced numerical model.

Preprints (www.preprints.org) | NOT PEER-REVIEWED | Posted: 29 July 2021 doi:10.20944/preprints202107.0672.v1

3.2. Example II

Figure 12 shows the vertical displacements of the PHC 40.0-9 slab obtained with the reference model due to prestressing. The maximum pre-bend obtained from the numerical model is 8.363 mm.

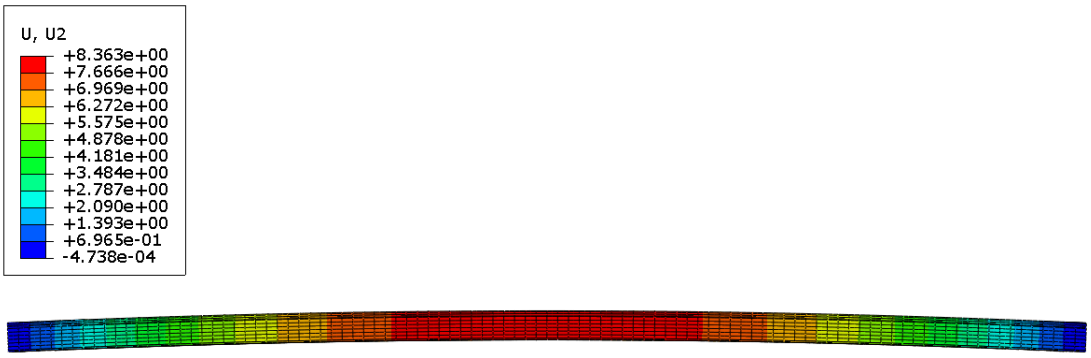

Fig. 12. Vertical displacement of the plate PHC 40.0-9 due to prestress.

Figure 13 shows plate deflections due to the combined effect of external load and prestress. The maximum deflection in the middle of the span for the PHC 40.0-9 plate and this type of load was 17.14 mm.

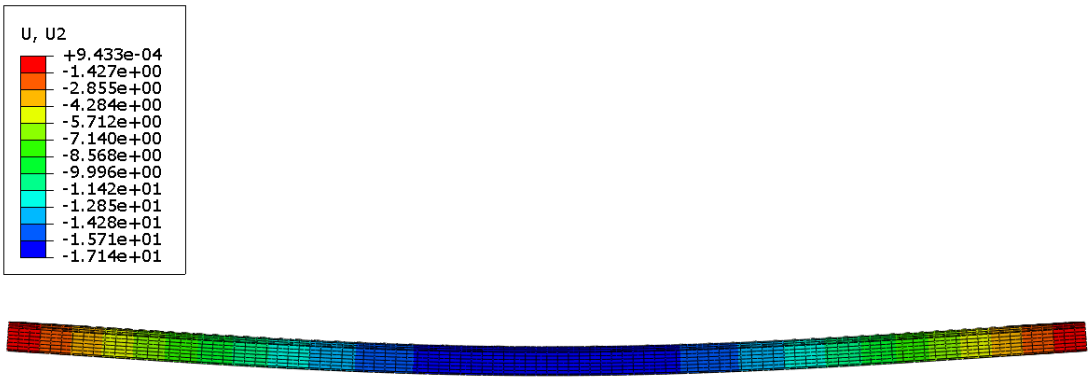

Fig. 13. Vertical displacement of the plate PHC 40.0-9 due to prestress and external load.

After performing the calculations using the FE-GNCL model, graphs of stiffness and vertical displacement were obtained for two load cases. Figure 14 shows the changes in stiffness along the length of the slab.

Preprints (www.preprints.org) | NOT PEER-REVIEWED | Posted: 29 July 2021 doi:10.20944/preprints202107.0672.v1

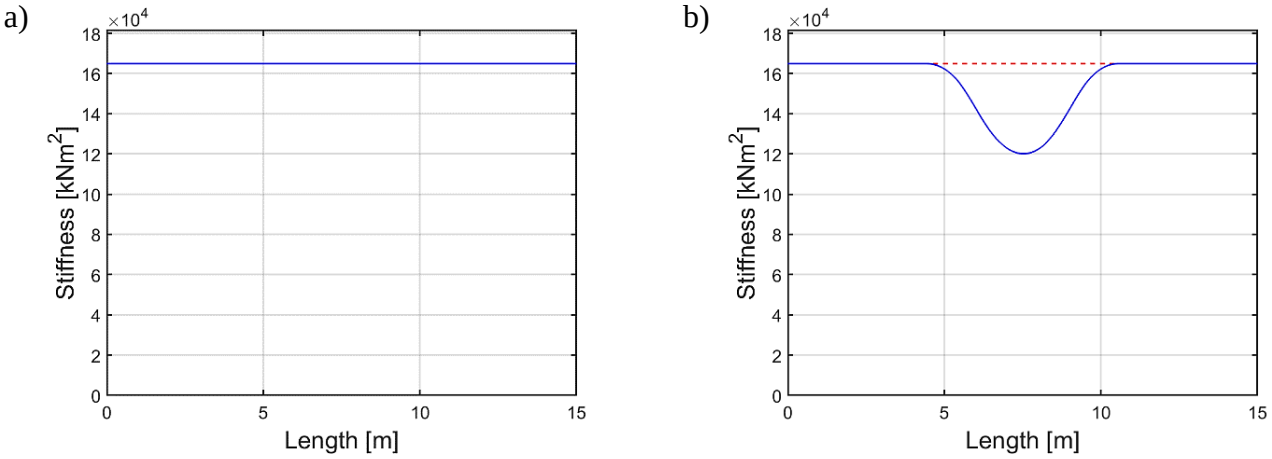

Fig. 14. The stiffness of the elements along the length of the plate PHC 40.0-9 due to: (a) prestress, (b) prestress and external load.

There was no change in the stiffness due to prestressing because the applied load was too small to obtain any plasticity of the panel cross section. For the combined action of prestressing and external load, the stiffness decreased by 27%. The maximum reduction is observed in the middle of the plate span, i.e. in the place where the highest values of the bending moment occurs. This is due to the fact that the value of curvature increases with increasing bending moments. This, in turn, causes the stiffness to change and decrease. In addition, the decrease in stiffness was caused by the use of the non-linear constitutive law both for concrete and steel.

Figure 15 shows the vertical displacements along the length of the slab caused by two kind of loading acting on the plate. In the case of prestressing only, a preliminary bend of 8.456 mm was obtained. For the joint action of the external load and prestress, the value of the maximum displacement in the middle of the span was 17.96 mm.

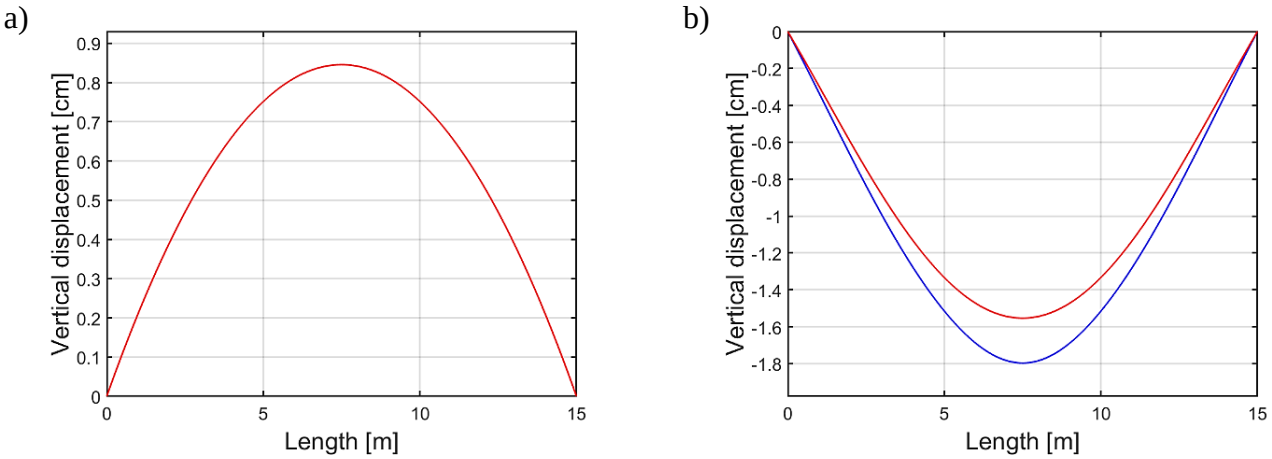

Fig. 15. Vertical displacement of the plate PHC 40.0-9 due to: (a) prestress, (b) prestress and external load.

Preprints (www.preprints.org) | NOT PEER-REVIEWED | Posted: 29 July 2021 doi:10.20944/preprints202107.0672.v1

Taking into account the nonlinear material model during the calculations resulted in an increase of displacements by 15.7% compared to the displacements obtained with the constant stiffness of the structure. It is worth noting that even a slight decrease in stiffness causes an increase in structure displacements by several percent.

The comparison of the obtained results from the three-dimensional reference FE-ABQ model and the simplified FE-GNCL model is presented in Table 4.

Table 4. Maximum vertical displacements of plate PHC 40.0-9.

	Reference model	GNCL model
Vertical displacement due to prestress [mm]	-8.363	-8.456
Vertical displacement due to prestress and external load [mm]	17.14	17.96

The results obtained from both models are very consistent. In the case of the maximum vertical displacements caused by the compression effect, the difference was just 1.1%, while for the combined effect of the external load and compression the difference increased to 4.7%. This confirms the validity of the simplified FE-GNCL model.

4. Conclusions

In the present work, the method based on the general nonlinear constitutive law for the strength analysis of prestressed hollow core slabs was presented. The applied GNCL method allows for easy consideration of material non-linearity and allows for the reduction of stiffness along the length of the element, caused by plasticization of steel or non-linear behaviour of concrete. Additionally, thanks to the use of the above method, it is possible to take into account the prestressing of the structure. Using the FE-GNCL model, it is possible to calculate complex cross-sections consisting of several materials with different physical properties.

In the benchmarks presented, two different examples of cross-sections of plates subjected to prestress and external load were analysed. The main advantage of the above method is that there is no need to build a complete and complicated 3D model with non-linear constitutive models of materials. This significantly facilitates the modelling of the structure and the calculation of the non-linear analysis. Knowledge and experience in this field is then not required. Moreover, the obtained results from the FE-GNCL model are consistent with the results obtained as a result of the three-dimensional analysis

of the reference FE-ABQ model built in commercial software Abaqus. In turn, the calculation time is significantly lower than in the case of the 3D model.

Additionally, on the basis of the analysed calculation examples, it can be concluded that the chosen physical laws of materials has a significant impact on the values of the plate displacements, and a slight decrease in stiffness already causes a significant increase in the vertical displacements of the structure. Moreover, the prestressing of the structure reduces the plate displacement under the influence of the external load.

The method presented in the above work obviously does not exhaust all the problems and topics related to the nonlinear strength analysis of the channelled prestressed plates. It is only an introductory work to the presented problem, which can be extended to a three-dimensional shell analysis using the FE-GNCL model.

References

[1] Abaqus Documentation Collection, Abaqus Analysis User's Manual, Abaqus/CAE User's Manual, 2020.

[2] A. Adawi, M. A. Youssef, M. E. Meshaly, „Finite element modeling of the composite action between hollow core slabs and the topping concrete", *Engineering Structures*, 124, pp. 302-315, Oct. 2016. doi: 10.1016/j.engstruct.2016.06.016

[3] A. Ajdukiewicz, K. Golonka, "Sprężone stropy płaskie dużej rozpiętości – środki techniczne, ograniczenia i metody projektowania", Konferencja Naukowo-Techniczna Konstrukcje Sprężone KS2015, Kraków, 16–17 kwietnia 2015, Editor: W. Derkowski, P. Gwoździkiewicz, M. Pańtak, W. Politelski, A. Seruga, M. Surma, *Materiały*, pp.11-38, 2015.

[4] D. P. Billington, "Historical Perspective on Prestressed Concrete", *PCI Journal*, 21(5), pp. 48–71, Sep.-Oct. 1976.

[5] T. Błaszczyński, B. Ksit, L. Grzegorczyk, "Nowa certyfikacja energetyczna jako element budownictwa zrównoważonego", *Wydawnictwo Politechniki Poznańskiej*, Poznan, Poland 2018.

[6] T. Clement, A. Pinho Ramos, M. F. Ruiz, A. Muttoni, "Design for punching of prestressed concrete slabs", *Structural Concrete*, 14(2), pp. 157-167, Jun. 2013. doi: 10.1002/suco.201200028

[7] W. Derkowski, "Nowe rozwiązania stropu sprężonego dla budynku hotelowo-konferencyjnego", *Czasopismo techniczne. Architektura*, 108(11), pp. 239-246, 2011.

[8] D. C. Drucker, W. Prager, "Soil mechanics and plastic analysis or limit design", *Quarterly of Applied Mathematics*, 10, pp. 157–165, 1952.

[9] R.C. Elstner , E.Hognestad, "Shearing strength of reinforced concrete slabs", *ACI Journal*, 53(1), pp. 29–58, 1956.

[10] T. Gajewski, T. Garbowski, "Calibration of concrete parameters based on digital image correlation and inverse analysis", *Archives of Civil and Mechanical Engineering*, 14, pp. 170-180, Jan. 2014. doi: 10.1016/j.acme.2013.05.012

[11] T. Gajewski, T. Garbowski, "Mixed experimental/numerical methods applied for concrete parameters estimation", Recent Advances in Computational Mechanics: proceedings of the 20th International Conference on Computer Methods in Mechanics (CMM 2013), Poznan, August, 2013, Editors: T. Łodygowski, J. Rakowski, P. Litewka, CRC Press/Balkema, pp. 293-302, 2014. doi: 10.1201/B16513

[12] T. Garbowski, G. Maier, G. Novati, "Diagnosis of concrete dams by flat-jack tests and inverse analyses based on proper orthogonal decomposition", *Journal of Mechanics of Materials and Structures*, 6 (1-4), pp. 181-202, Jan.-Jun. 2011. doi: 10.2140/JOMMS.2011.6.181

[13] J. van Greunen, A. C. Scordelis, "Nonlinear analysis of prestressed concrete slabs", *Journal of Structural Engineering*, 109, pp. 1742-1760, 1983.

[14] I. Holly, I. Abrahoim, L. Fillo, "3D Nonlinear Analysis of Precast Prestressed Hollow Core Slab", *IOP Conference Series: Materials Science and Engineering* WMCAUS 15-19 June 2020, Prague, Czech Republic, vol. 960, 2020.

[15] T. N. Hang Nguyen, K. Tan, T. Kanda, "Investigations on web-shear behaviour of deep precast, prestressed concrete hollow core slabs", *Engineering Structures*, 183, pp. 579-593, Mar. 2019. doi: 10.1016/j.engstruct.2018.12.052

[16] I. S. Ibrahim, K. S. Elliott, R. Abdullah, A. B. H. Kueh, N. N. Sarbini, "Experimental study on the shear behaviour of precast concrete hollow core slabs with concrete topping", *Engineering Structures*, 126, pp. 80-90, Oct. 2016. doi: 10.1016/j.engstruct.2016.06.005

[17] T. Jankowiak, T. Łodygowski, "Identification of parameters of concrete damage plasticity constitutive model", *Foundations of Civil and Environmental Engineering*, No. 6, pp. 53-69, 2005.
[18] M. Knauff, "Podstawy projektowania konstrukcji żelbetowych i sprężonych według Eurokodu 2", *Dolnośląskie Wydawnictwo Edukacyjne* , Wrocław, Poland, 2006.
[19] F. Liu, J. Battini, C. Pacoste, A. Granberg, "Experimental and Numerical Dynamic Analyses of Hollow Core Concrete Floors", Structures, 12, pp. 286-297, Nov. 2017. doi: 10.1016/j.istruc.2017.10.001
[20] "MATWORK" https://www.mathworks.com/help/matlab/ (dostęp 28.06.2021r.)
[21] G. Maier, G. Bolzon, V. Buljak, T. Garbowski, B. Miller, "Synergic Combinations of Computational Methods and Experiments for Structural Diagnoses", in Computer Methods in Mechanics. Advanced Structured Materials; Eds. M. Kuczma, K. Wilmanski, *Springer*, Berlin/Heidelberg, Germany, pp. 453–476, 2010. doi: 10.1007/978-3-642-05241-5_24
[22] D. Mrówczyński, T. Gajewski, T. Garbowski, "Application of the generalized nonlinear constitutive law in 2D shear flexible beam structures". Preprints 2021, 2021060178. doi: 10.20944/preprints202106.0178.v1.
[23] D. Mrówczyński, T. Gajewski, T. Garbowski, "The generalized constitutive law in nonlinear structural analysis of steel frames", in Modern Trends in Research on Steel, Aluminium and Composite Structures; Eds. M. A. Giżejowski, A. Kozłowski, M. Chybiński, K. Rzeszut, R. Studziński, M. Szumigała, *Routledge Taylor and Francis Group,* pp. 120-125, 2021. doi: 10.1201/9781003132134-12
[24] Poradnik projektanta Strunobetonowe płyty stropowe kanałowe HC, Consolis, Gorzkowice, Poland, 2010
[25] PN-EN 1992-1-1:2008 - Eurocode 2: Design of concrete structures - Part 1-1: General rules, and rules for buildings, 2008.
[26] E. Radziszewska-Zielina, "Fuzzy control of the partnering relations of a construction enterprise", *Journal of Civil Engineering and Management*, 17(1), pp. 5-15, 2011. doi: 10.3846/13923730.2011.554172
[27] A. Rodrigeus da Silva, J. Paulo de Souze Rosa, "Nonlinear numerical analysis of prestressed concrete beams and slabs", *Engineering Structures*, 223, Nov. 2020. doi: 10.1016/j.engstruct.2020.111187
[28] G. Sathurappan, N. Rajogopalan, C. S. Krishnamoorthy, "Nonlinear finite element analysis of reinforced and prestressed concrete slabs with reinforcement (inclusive of prestressing steel) modelled as discrete integral components", *Computers & Structures*, 44(3), pp.575-584, 1992
[29] A. M. Shakya, V. K. R. Kodur, "Response of precast prestressed concrete hollowcore slabs under fire conditions", *Engineering Structures*, 87, pp. 126-138, Mar. 2015. http://dx.doi.org/10.1016/j.engstruct.2015.01.018
[30] N. Staszak, T. Gajewski, T. Garbowski, "Generalized nonlinear constitutive law applied to steel trapezoidal sheet plates", in Modern Trends in Research on Steel, Aluminium and Composite Structures; Eds. M. A. Giżejowski, A. Kozłowski, M. Chybiński, K. Rzeszut, R. Studziński, M. Szumigała, Routledge Taylor and Francis Group, pp. 185-191, 2021. doi: 10.1201/9781003132134-21
[31] W. Starosolski, "Konstrukcje żelbetowe według PN-B-03264:2002 i Eurokodu 2", tom I, Wyd. 12, *Wydawnictwo Naukowe PWN*, Warszawa, Poland, 2009.
[32] T. Steinar, "Structural Behaviour of Post Tensioned Concrete Structures: Flat Slab. Slabs on Ground", Doctoral thesis, Fakultet for ingeniørvitenskap og teknologi, Trondheim, Norwegia, 2001.
[33] M. Szumigała, "Zespolone stalowo-betonowe konstrukcje szkieletowe pod obciążeniem doraźnym", Wydawnictwo Politechniki Poznańskiej, Poznan, Poland, 2007.
[34] R. Szydłowski, "Concrete properties for long-span post-tensioned slabs", 2nd International Symposium on Advanced Material Research (ISAMR 2018), Jeju Island, Republic of Korea, March 16th-18th, 2018 and Materials Science Forum, Vol. 296, pp. 122–127, Jul. 2018. doi: 10.4028/www.scientific.net/MSF.926.122

 doi:10.20944/preprints202107.0672.v1

Zastosowanie uogólnionego nieliniowego prawa konstytutywnego dla kanałowych płyt stropowych

Słowa kluczowe: *uogólnione nieliniowe prawo konstytutywne, analiza elementu skończonego, nieliniowość materiałowa, kompozyt, element płytowy Reissnera-Mindlina*

Streszczenie: Nieliniowa analiza kanałowych płyt stropowych wymaga zastosowania zaawansowanych technik numerycznych, odpowiednich modeli konstytutywnych zarówno dla betonu jak i stali oraz konieczności posiadania odpowiednich umiejętności obliczeniowych. W przypadku nieliniowych analiz należy wziąć pod uwagę również sprężenie, pękanie, rysy, zmiękczenie materiału itp., co powoduje że zadanie obliczeniowe może znacznie przekroczyć możliwości zwykłego inżyniera. W celu wykonania obliczeń w tradycyjnym biurze projektowym potrzebne są uproszczone metody obliczeń. Najlepiej w oparciu o liniową metodę elementów skończonych (MES) z prostym podejściem uwzględniającym nieliniowości materiałowe. W artykule przedstawiono uproszczoną analizę kanałowych płyt w oparciu o uogólnione prawo konstytutywne. W proponowanej metodzie prosty rozkład tradycyjnej iteracyjnej liniowej analizy elementów skończonych oraz nieliniowej analizy algebraicznej przekroju poprzecznego płyty. Poprzez niezależną analizę przekroju płyty w różnych stanach odkształcenia, można uzyskać zdegradowaną sztywność płyty, co pozwala na iteracyjną aktualizację przemieszczeń oraz obrotów w węzłach modelu MES. To z kolei pozwala zaktualizować stan deformacji, a następnie skorygować translacje i obroty w węzach jeszcze raz. Proponowana tutaj metoda ma zastosowanie do analizy betonu zbrojonego cięgnami oraz sprężonych płyt kanałowych. Wyniki uzyskane z pełnego szczegółowego nieliniowego modelu 3D MES oraz z proponowanego podejścia są porównywane dla różnych przekrojów płyt. Uzyskane wyniki dają dobrą zbieżność.